CHEMISTRY OF MATERIALS

Article

pubs.acs.org/cm

General Strategy for Zero-Valent Intercalation into Two-Dimensional Layered Nanomaterials

Janina P. Motter,[†] Kristie J. Koski,[‡] and Yi Cui*[,†,§]

[†]Department of Materials Science and Engineering, Stanford University, Stanford, California 94305, United States

[‡]Department of Chemistry, Brown University, Providence, Rhode Island 02912, United States

[§]SLAC National Accelerator Laboratory, Stanford Institute for Materials and Energy Sciences, 2575 Sand Hill Road, Menlo Park, California 94025, United States

Supporting Information

ABSTRACT: We demonstrate the complete tunability of a general strategy to intercalate zero-valent atoms into two-dimensional (2D) layered materials. A chemical method was used to intercalate high densities of copper (up to 55 atomic percent) into synthesized nanomaterials such as MoO_3, Sb_2Te_3, In_2Se_3, and GaSe. These materials were characterized using TEM, EDX, electron diffraction, XRD, Raman, EELS, and XPS to observe the effects of intercalation, determine the concentration of copper, and confirm the zero-valent nature of the intercalant as well as unchanged structure of the host material. This technique reveals the power and potential to observe unique chemical and physical phenomena and to control such properties for particular applications.

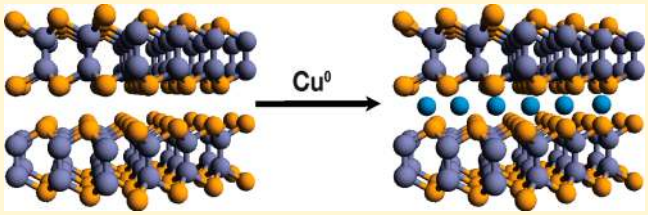

Two-dimensional (2D) layered materials have recently attracted much interest due to their unique physical and chemical properties[1,2] and myriad applications in areas such as electronics, electrochemical energy storage,[3,4] and catalysis.[5] Unique chemical and physical phenomena can be controllably tuned by nanostructuring,[6] exfoliation,[7] or intercalation of molecules, atoms, and ions between the layers of these structures. In particular, effects such as charge density waves,[8] anisotropic transport properties,[9] spontaneous magnetization,[10] 2D electron-gas physics,[11] and superconductivity[12] have already been demonstrated and can be potentially tuned. Traditionally, charged species have been inserted into these materials, which limits the intercalant concentration due to the requirement of the change in oxidation state in host materials. In order to establish fundamentally new and unexpected physical behaviors, or to generate new methods of atomic storage for potential energy or catalytic materials applications, we previously demonstrated a solution-based method to intercalate zero-valent copper into Bi_2Se_3 nanoribbons.[13] This simple and versatile route was able to preserve the morphology and structure of the host material, resulting in high densities (up to 60 atomic percent copper, $Cu_{7.5}Bi_2Se_3$) of intercalant concentration that had never been previously achieved. Furthermore, this strategy was shown to be general in Bi_2Se_3 nanoribbons when extending to other zero-valent guest species such as Ag, Au, Co, Fe, In, Ni, and Sn.[14] However, it is not yet known whether such superstoichiometric ($x > 1$), zero-valent intercalation can be extended to different 2D host materials.[15] If demonstrated, this would open up many exciting opportunities of accessing interesting chemical and physical properties.

In this study, we demonstrate that this method can be further extended to other layered materials, including MoO_3, Sb_2Te_3, In_2Se_3, and GaSe (Figure 1). MoO_3 has applications in electrochromic devices .[16] Nanostructured Sb_2Te_3 has potential use as a high-ZT thermoelectric material. Due to its large

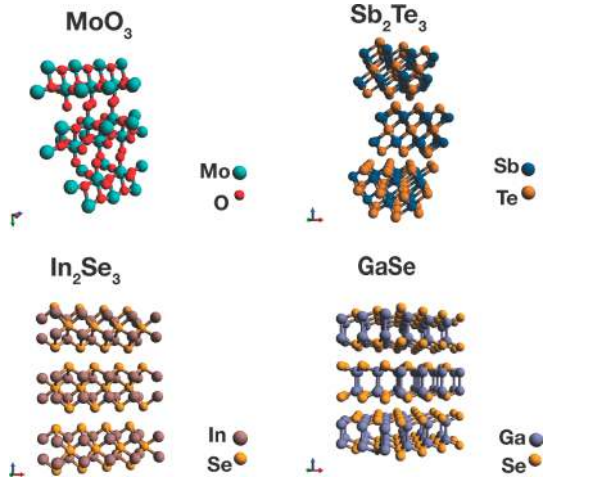

Figure 1. Crystal structures of the 2D layered materials explored in this study.[18] These materials consist of layers separated by van der Waals gaps that can host intercalant copper atoms. Space group and unit cell parameters are provided in the Experimental section.

Received: January 21, 2014
Revised: March 10, 2014

   dx.doi.org/10.1021/cm500242h | Chem. Mater. XXXX, XXX, XXX−XXX

bonding anisotropy, In_2Se_3 has potential applications in batteries, solar cells, and phase change memory devices.[17] The high level of bonding anisotropy in GaSe suggests applications such as solar cells, nonlinear optics, or solid-state batteries.

Using characterization tools such as in situ transmission electron microscopy (TEM), electron diffraction, energy dispersive X-ray (EDX) spectroscopy, electron energy loss spectroscopy (EELS), X-ray photoelectron spectroscopy (XPS), Raman, and X-ray diffraction (XRD), we determine the concentration of copper intercalant and confirm the unchanged composition of each host material, as well as the zero-valent state of the intercalant. We suggest a fully customizable template to intercalate high densities of zero-valent atoms into a layered host material, with the choice determined by specific application and the possibility for radically new and unexpected chemistry and physics.

EXPERIMENTAL SECTION

Synthesis. *MoO_3 Nanowires.* MoO_3 (M_w = 143.94 g/mol) crystallizes in the orthorhombic system with space group *Pbnm*, lattice parameters a = 3.962 Å, b = 13.858 Å, c = 3.697 Å, and Z = 4. Nanowires 100 nm wide, 10 nm thick, and tens of micrometers long were prepared using the solvothermal synthesis of Li et al.[19] Metallic molybdenum powder (0.36 g) was added into 30 mL distilled water with shaking. Then, 2.5 mL of 30% H_2O_2 was added dropwise, and the reaction was allowed to stir for 20 min. The mixture was sealed in an autoclave and maintained at 150 °C for 12 h. Products were washed with distilled water.

Sb_2Te_3 Nanoplates. Sb_2Te_3 (M_w = 626.30 g/mol) crystallizes in the rhombohedral system with space group $R\bar{3}m$, lattice parameters $a = b$ = 4.262 Å and c = 30.45 Å, and Z = 3. Nanoplates approximately 500 nm in diameter were prepared following a modified version of the synthesis of Zhou et al.[20] Briefly, 2 mmol antimony sodium tartrate ($Na(SbO)C_4H_4O_6$), 3 mmol Te powder, 2 g of NaOH, 0.5 g PVP, and 30 mL of ethylene glycol were combined and allowed to stir for 2 h. The solution was sealed in an autoclave and maintained at 165 °C for 72 h, then allowed to cool to room temperature. Products were washed with ethanol and distilled water and left in solution of acetonitrile overnight to remove excess reactants.

In_2Se_3 Nanoribbons. In_2Se_3 (M_w = 466.52 g/mol) crystallizes in the hexagonal system with space group $P6_3/mmc$, lattice parameters $a = b$ = 4.025 Å and c = 19.235 Å, and Z = 2. VLS In_2Se_3 ribbons were prepared using a method developed previously by our group,[21] with polycrystalline In_2Se_3 as source powder and source temperature of 700 °C maintained for 4 h.

GaSe Nanoribbons. GaSe (M_w = 148.69 g/mol) crystallizes in the hexagonal system with space group $P6_3/mmc$, lattice parameters $a = b$ = 3.742 Å, c = 15.919 Å. GaSe nanobelts were prepared following a modified version of the vapor−liquid−solid (VLS) growth method of Peng et al.[22] Quartz substrates were covered with 20 nm diameter Au particles and placed downstream in a 12 in. horizontal tube furnace (Lindberg/Blue M) equipped with a 1 in. diameter quartz tube, with source polycrystalline GaSe powder in the middle of the furnace. High-purity N_2 premixed with 2%H_2 (99.999%) acted as a carrier gas. The tube was repeatedly flushed with the carrier gas at 150 mTorr to decrease oxygen contamination, and maintained at 115 sccm at a pressure of 1 atm during growth. The source temperature was ramped to 800 °C at a rate of 70 °C/min, and maintained for 3 h.

Cu Intercalation. In a typical reaction, the source material was added to a 10 mM solution of tetrakis(acetonitrile) copper(I) hexafluorophosphate in acetone and kept just under reflux (at 45 °C) for four hours. Prior to the reaction, glassware is cleaned in an acid bath and soaked overnight in acidic distilled water to adjust the pH to 4 to 6.5.

Characterization. The elemental composition, structure, lattice constants, and oxidation state of the intercalant were confirmed with several characterization tools. In situ transmission electron microscopy (TEM), diffraction, images, and energy dispersive X-ray (EDX) spectroscopy were acquired on single nanostructures on a FEI Tecnai G2 F20 at 200 keV with a Gatan double-tilt heating holder. Electron energy loss spectroscopy (EELS) was performed on the same instrument operated at 200 keV. Raman spectra were collected using a WiTec Alpha 500 Spectrometer System with a laser excitation of 532 nm. X-ray diffraction (XRD) data was acquired using a PANalytical X'Pert Pro 2 using Cu Kα X-ray radiation source (1.54 Å) by performing a 2θ to ω scan at 45 kV and 40 mA. X-ray photoelectron spectroscopy (XPS) data was collected with a PHI VersaProbe Scanning XPS Microbe using Al Kα radiation (1486 eV), with source material on a silicon substrate.

RESULTS AND DISCUSSION

We intercalated into several layered nanomaterial oxides and chalcogenides (MoO_3, In_2Se_3, Sb_2Te_3, and GaSe).

TEM images before and after Cu atom intercalation are shown in Figure 2, revealing that the morphology is preserved.

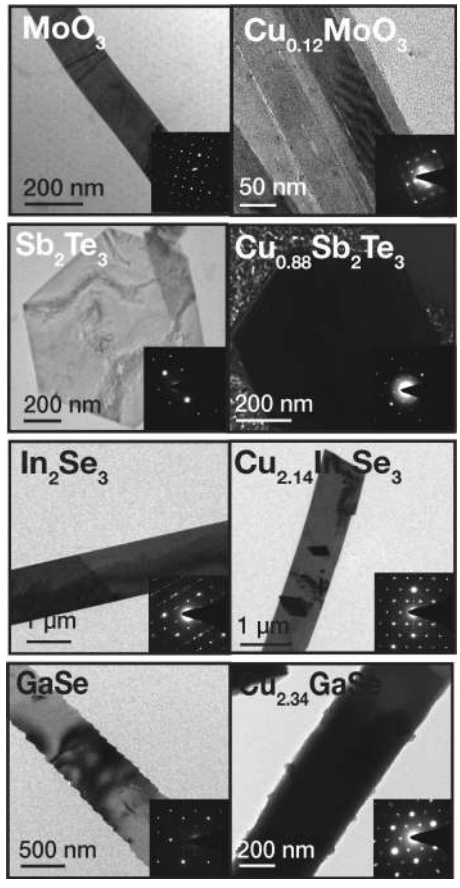

Figure 2. TEM images (including SAED diffraction patterns) for materials before and after Cu^0 intercalation.

No particulates or aggregates of copper are seen on the nanowires. No polycrystalline diffraction rings are observed in the electron diffraction patterns, confirming absence of nanoparticle aggregates. The stripe-like phase of a charge density wave is also visible in the intercalated MoO_3 wires (Figure 2).

The amount of copper was quantified using EDX (Supporting Information; Figure S1). Table 1 provides the maximum atomic percentage of zero-valent copper intercalated into the various nanomaterials using a 10 mM solution of precursor copper (I) salt in acetone held at reflux for four

dx.doi.org/10.1021/cm500242h | Chem. Mater. XXXX, XXX, XXX−XXX

Table 1. Maximum Atomic Percentage of Zero-Valent Copper Intercalated into Synthesized Materials Using a 10 mM Solution of Cu Precursor in Acetone

structure	intercalated compound stoichiometry	atomic percent of Cu^0 intercalation
MoO_3	$Cu_{0.12}MoO_3$	3
Sb_2Te_3	$Cu_{0.88}MoO_3$	15
In_2Se_3	$Cu_{2.14}In_2Se_3$	28.79
GaSe	$Cu_{2.34}GaSe$	54.60

hours. Highest intercalation concentrations are observed in the selenides. For comparison, up to 60 atomic percent of copper can be intercalated into Bi_2Se_3 nanoribbons under similar reaction conditions.[23]

In previous work, at high enough densities of Cu intercalation, superlattice patterns could be observed in the selected area electron diffraction (SAED) patterns collected using TEM.[13] Superlattice patterns indicative of copper intercalant ordering are also seen here in In_2Se_3 and GaSe (Figure 2). Both show a hexagonal pattern of ordering similar to our previous observations of copper intercalated Bi_2Se_3 (Supporting Information; Figure S2). Diffraction patterns are observed by looking down a 3-fold symmetry axis. A superlattice will have a subset of those crystal symmetries and will also be 3-fold. The simplest Bravais lattice with 3-fold rotational symmetry is hexagonal, which explains the consistency in observation of a hexagonal superlattice pattern for these host crystal structures.

Using XRD, the contraction or expansion of the unit cell volume due to intercalation was observed for MoO_3, Sb_2Te_3, and In_2Se_3 (Figure 3). Assignment of the peaks also confirmed that the expected structures of the host materials had been synthesized. For MoO_3, the *b* lattice parameter, dictated by layer spacing and calculated from the (060) peak, shifts from 13.931 Å to 13.856 Å with copper intercalation. This corresponds to a lattice *d*-spacing shift from 2.322 Å (38.783°) to 2.309 Å (39.004°). The observed peaks match earlier conclusions of (0*k*0) characteristic diffraction peaks of MoO_3 and the preferred orientation of the sample.[24] For Sb_2Te_3, the *c* lattice parameter, calculated from the (006) peak, shifts from 33.306 Å to 33.221 Å. This corresponds to a *d*-spacing shift from 5.551 Å (15.966°) to 5.537 Å (16.0065°). Additional peaks were observed in Sb_2Te_3 diffraction patterns (marked with an asterisk), which likely result from unreacted Te still present in the sample. These peaks did not follow the trend of shifted lattice parameter to match contraction of the lattice. The shift in *c* lattice parameter from 18.795 Å to 18.805 Å with copper intercalation was observed for In_2Se_3 (calculated from the (004) peak). This corresponds to a *d*-spacing shift from 4.699 Å (18.886°) to 4.701 Å (18.876°). Because of low sample volume and since large variations in crystallinity exist between different substrates of prepared GaSe, XRD was not performed. With varying amounts of intercalant, we see both contraction and expansion in the lattice. This has been observed previously with other intercalant systems.[25] In particular, since contraction has previously been associated with acceptor intercalants, we suspect that the Cu-intercalated MoO_3 is "low-valent" and exhibits some electron sharing, as discussed further below.[26] For the case of Sb_2Te_3, the presence of excess unreacted metal may have limited the intercalation reaction, as the Te could have occupied some of the available space in the van der Waals gaps.[27]

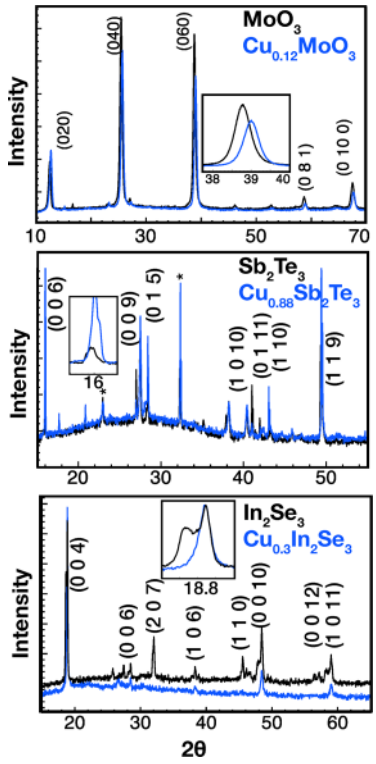

Figure 3. XRD spectra for MoO_3, Sb_2Te_3, and In_2Se_3 before and after Cu intercalation. The inset of MoO_3 demonstrates the peak shift of the (060) peak. Similar shifts are present in Sb_2Te_3 (inset of (006) peak) and In_2Se_3 (inset of (004) peak).

Intercalation was further confirmed by the shift in peaks observed using Raman spectroscopy (Figure 4). The bulk spectra of GaSe was obtained from the precursor synthesis powder. The bulk spectra of MoO_3 was obtained from a database of bulk mineral samples, as compared to the synthesized materials in this study.[28] Additionally, the different

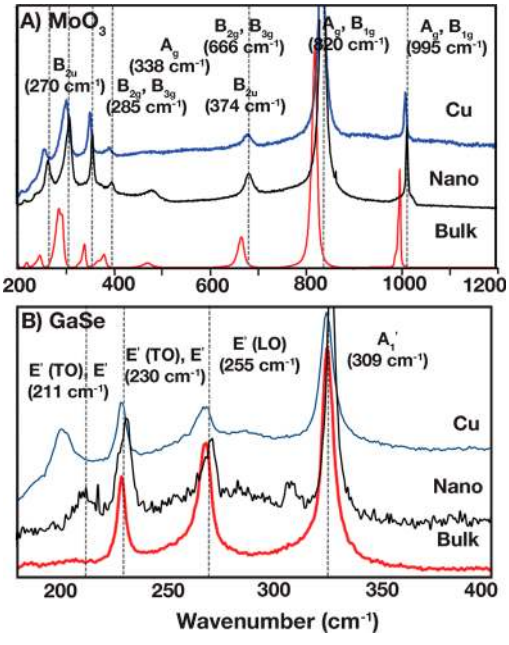

Figure 4. Raman spectra for MoO_3 and GaSe, demonstrating the unique peak shifts due to intercalation.

dx.doi.org/10.1021/cm500242h | *Chem. Mater.* XXXX, XXX, XXX−XXX

experimental setup further explains the shift in peaks from the bulk to the nano samples in each case.

For MoO_3 (Figure 4A), several peaks corresponding to asymmetric stretches and wagging modes of the terminal oxygens[29,30] shifted to lower wavenumber values. In particular, the A_g (354.96 to 353.87 cm^{-1} and 1012.90 to 1008.09 cm^{-1}, corresponding to the symmetric stretch and vibration of the terminal oxygen atoms), B_{2u} (262.49 to 260.11 cm^{-1} and 394.90 to 392.60 cm^{-1}, representative of asymmetric stretches of the terminal oxygen atoms), and B_{2g} and B_{3g} (305.32 to 302.56 cm^{-1}, corresponding to asymmetric stretches of the terminal oxygen atoms) modes shifted to lower wavenumber values. No change was observed for the modes associated with the O−Mo−O bridging oxygen atom stretches at 666 and 820 cm^{-1}.

As the intercalated atoms sit between layers, the terminal oxygen groups in the MoO_3 structure have less space, resulting in less vibrational freedom. The shift in these frequencies indicates interaction between the copper intercalant and these oxygen atoms sitting within the van der Waals gap of the MoO_3 host. The interlayer modes are located below detection frequencies of the instrument used for this study.

Given that the characteristic Raman modes are observed below 200 cm^{-1}, it was not possible to characterize Sb_2Te_3 or In_2Se_3 with the experimental setup used.[31] The spectra for GaSe (4B) showed similar shifts of the A_1^1 and E′ peaks to lower energy after Cu intercalation, which both correspond to vibrations within the covalently bound layers. Given the restricted motion of the atoms after extensive intercalation, it makes sense that less energy was required for these vibrational frequencies.[32−35]

As in our previous studies on Bi_2Se_3,[13,14] EELS fine structure and XPS measurements were used to confirm the zero-valent nature of the copper intercalant. Fine structure plots for In_2Se_3 and GaSe are shown in Figure 5, along with reference plots for

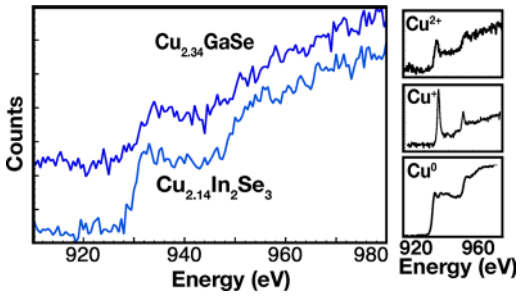

Figure 5. EELS fine structure plots, confirming the zero-valent nature of the intercalated copper.

Cu^0, Cu^+, and Cu^{2+}. No sharp peaks are observed (as seen in mono- and divalent copper) in the samples, and the peak pattern closely matches that of zero-valent copper. It should be noted that the nanoribbon tested using EELS for zero-valency was the same that is shown in Figure 2.

The EELS fine structure for MoO_3 was a unique case, as the observed peak appears to be a mix of the Cu^0 and Cu^{2+} fine structures (Figure 6).

As shown in Figure 5, Cu^{2+} and Cu^+ exhibit sharp L_2 and L_3 edges, whereas Cu^0 shows only broad edges due to its completely filled 3*d* band.[36] The EELS fine structure plot for $Cu_{0.12}MoO_3$ (Figure 6B) shows a noticeably sharp L_3 edge (like Cu^{2+}), but the peak is also clearly broadened (as in Cu^0). This

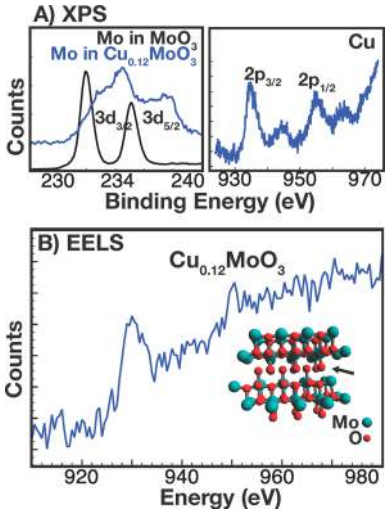

Figure 6. EELS fine structure plots and XPS binding energies exhibiting the electron sharing that likely occurs between O and Cu in intercalated MoO_3.

is further evidenced by the shift in Mo binding energy and broader satellite peaks (at approximately 940 and 960 eV)[37] observed in the Cu binding energy measurement with XPS. Satellite peaks are characteristic of Cu^{2+} structures. At the same time, the Cu $p_{3/2}$ peak has been shown to broaden with increase in oxidation state from Cu^0 to Cu^{2+}, as well as increase to higher values.[38] In particular, an extremely broad peak (fwhm = 3.8, similar to this sample) has previously been evidence of multiple valence states with overlapping peaks, so we suspect that copper exists in different environments within the structure, likely due to the presence of terminal oxygen atoms within the van der Waals gap where the copper is intercalated.

The structure of MoO_3 (Figure 1) consists of molybdenum atoms bound in a distorted octahedral configuration by both bridging oxygen atoms and nonbridging oxygen atoms. Nonbridging oxygen atoms extend toward the van der Waals gap between successive layers. Materials intercalated into the van der Waals gap of MoO_3 will have increased interaction with these nonbridging oxygen atoms. This also makes the van der Waals gap smaller than other selenide and telluride materials studied in this work.

EDX was used to quantify the atomic percentage of copper (Supporting Information; Figure S1). A constant ratio of the intensity of Sb/Te peaks as 0.84 before and after intercalation was confirmed. The intensity ratio of In/Se also remained constant before and after intercalation. It was difficult to quantify a constant ratio of Mo/O before and after intercalation given the large quantities of oxygen present in ambient conditions.

We have previously outlined the disproportionation of monovalent copper under the reaction conditions to zero-valent and divalent species.[13] We proposed that zero-valent intercalation is thermodynamically and possibly kinetically favored (over nucleation of nanoparticles in solution) due to the low concentrations of metal atoms generated and their limited solubility in organic solvents.[14] There are several different components that can affect the amount of copper intercalated into the samples, including the duration of intercalation and the concentration of copper precursor salt relative to nanomaterial. For example, in solvothermally or

dx.doi.org/10.1021/cm500242h | Chem. Mater. XXXX, XXX, XXX−XXX

hydrothermally prepared materials, there will almost always be some of the precursor water or ethylene glycol in the van der Waals gap, which affects the amount of copper that can be intercalated in, since it alters the environment and takes up space. Another factor is the nature of the van der Waals gap itself. For example, in MoO_3, the oxygen atoms sit in the van der Waals gap and can interact with the copper intercalant, preventing large amounts of uptake. The number of defects and the nature of the edges of the nanomaterial also likely play a role.

CONCLUSION

We have demonstrated that the previously reported chemical method to intercalate high densities (up to 55 atomic percent) of zero-valent Cu atoms is general by intercalating into a variety of layered materials, including MoO_3 ($Cu_{0.12}MoO_3$), Sb_2Te_3 ($Cu_{0.88}Sb_2Te_3$), In_2Se_3, ($Cu_{2.14}In_2Se_3$), and GaSe ($Cu_{2.34}GaSe$). Precipitates were not observed in TEM, either visibly or within the diffraction patterns. Superlattice patterns were observed for materials with atomic percentages of copper greater than 15%. The morphology of each material was preserved after intercalation. XRD spectra demonstrate contraction and expansion of the unit cell as a result of intercalation. Raman results demonstrate peak shifts as a result of intercalation. EELS fine structure and XPS measurements confirm the intercalated Cu is of zero-valent nature. Additionally, the intensity ratios of Sb/Te and In/Se, remained constant before and after intercalation, confirming that the presence of Cu atoms does not disrupt the host structure.

Combined with our previously reported technique to intercalate different zero-valent metal atoms into layered structures, we have proposed a general template to intercalate zero-valent atoms into different layered materials and tune the process for the desired chemical or physical properties. This offers potential impact to generate fundamentally new and unexpected behaviors and serves as a novel form of atomic storage for possible energy or catalytic materials applications.

ASSOCIATED CONTENT

Supporting Information

EDX spectra of all materials before and after Cu intercalation. SAED diffraction patterns exhibiting superlattices in intercalated In_2Se_3 and GaSe. This material is available free of charge via the Internet at http://pubs.acs.org.

AUTHOR INFORMATION

Corresponding Author

*E-mail: yicui@stanford.edu.

Notes

The authors declare no competing financial interest.

ACKNOWLEDGMENTS

We acknowledge support by the Department of Energy, Office of Basic Energy Sciences, Materials Sciences and Engineering Division, under contract DE-AC02-76-SFO0515.

REFERENCES

(1) Geim, A. K. *Science* **2009**, *324*, 1530−1534.
(2) Geim, A. K.; Novoselov, K. S. *Nat. Mater.* **2007**, *6*, 184−191.
(3) Whittingham, M. S. *J. Solid State Chem.* **1979**, *29*, 303−310.
(4) Tarascon, J.-M.; Armand, M. *Nature* **2001**, *414*, 359−367.
(5) Kibsgaard, J.; Chen, Z.; Reinecke, B. N.; Jaramillo, T. F. *Nat. Mater.* **2012**, *11*, 963−969.
(6) Mehta, R. J.; Zhang, Y.; Karthik, C.; Singh, B.; Siegel, R. W.; Borca-Tasciuc, T.; Ramanath, G. *Nat. Mater.* **2012**, *11*, 233−240.
(7) Coleman, J. N.; et al. *Science* **2011**, *331*, 568−571.
(8) Wilson, J. A.; Di Salvo, F. J.; Mahajan, S. *Adv. Phys.* **1975**, *24* (2), 117−201.
(9) Patzke, G. R.; Krumeich, F.; Nesper, R. *Angew. Chem., Int. Ed.* **2002**, *41*, 2446−2461.
(10) Prellier, W.; Singh, M. P.; Murugavel., P. *J. Phys.: Condens. Matter* **2005**, *17*, R803−R832.
(11) Berger, C.; Song, Z.; Li, T.; Li, X.; Ogbazghi, A. Y.; Feng, R.; Dai, Z.; Marchenkov, A. N.; Conrad, E. H.; First, P. N.; de Heer, W. A. *J. Phys. Chem. B* **2004**, *108*, 19912−19916.
(12) Hor, Y. S.; Checkelsky, J. G.; Qu, D.; Ong, N. P.; Cava, R. J. *J. Phys. Chem. Solids* **2011**, *72*, 572−576.
(13) Koski, K. J.; Cha, J. J.; Reed, B. W.; Wessells, C. D.; Kong, D.; Cui, Y. *J. Am. Chem. Soc.* **2012**, *134*, 7584−7587.
(14) Koski, K. J.; Wessells, C. D.; Reed, B. W.; Cha, J. J.; Kong, D.; Cui, Y. *J. Am. Chem. Soc.* **2012**, *134*, 13773−13779.
(15) Ganal, P.; Moreau, P.; Ouvrard, G.; Sidorov, M.; McKelvy, M.; Glaunsinger, W. *Chem. Mater.* **1995**, *7*, 1132−1139.
(16) Tang, J.; Lu, Y.; Liu, B.; Yang, P.; Huang, Y.; Kong, J. *J. Solid State Electrochem.* **2003**, *7*, 244−248.
(17) Peng, H.; Xie, C.; Schoen, D. T.; Cui, Y. *Nano Lett.* **2008**, *8* (5), 1511−1516.
(18) Avogadro: an open-source molecular builder and visualization tool. Version 1.1.0. http://avogadro.openmolecules.net/ (accessed May 21, 2013).
(19) Li, G.; Jiang, L.; Pang, S.; Peng, H.; Zhang., Z. *J. Phys. Chem. B* **2006**, *110*, 24472−24475.
(20) Zhou, B.; Ji, Y.; Yang, Y.-F.; Li, X.-H.; Zhu, J.-J. *Cryst. Growth Des.* **2008**, *8* (12), 4394−4397.
(21) Peng, H.; Schoen, D. T.; Meister, S.; Zhang, X. F.; Cui, Y. *J. Am. Chem. Soc.* **2007**, *129*, 34−35.
(22) Peng, H.; Meister, S.; Chan, C. K.; Zhang, X. F.; Cui., Y. *Nano Lett.* **2007**, *7* (1), 199−203.
(23) Koski, K. J.; Cha, J. J.; Reed, B. W.; Wessells, C. D.; Kong, D.; Cui, Y. *J. Am. Chem. Soc.* **2012**, *134*, 7584−7587.
(24) Cai, G. M.; Jian, J. K.; Chen, X. L.; Lei, M.; Wang, W. Y. *Appl. Phys. A: Mater. Sci. Process.* **2007**, *89*, 783−788.
(25) Dresselhaus, M. S.; Dresselhaus, G. *Adv. Phys.* **2002**, *51*, 1−186.
(26) Sidorov, M.; McKelvy, M.; Sharma, R.; Glaunsinger, W.; Ganal, P.; Moreau, P.; Ouvrard, G. *Chem. Mater.* **1995**, *7*, 1140−1152.
(27) Friend, R. H.; Yoffe, A. D. *Adv. Phys.* **1987**, *36* (1), 1−94.
(28) Downs, R. T. *Program and Abstracts of the 19th General Meeting of the International Mineralogical Association*, Kobe, Japan, 2006.
(29) Sequin, L.; Figlarz, M.; Cavagnat, R.; Lassègues, J.-C. *Spectrochim. Acta Part A* **1995**, 1323−1344.
(30) Windom, B. C.; Sawyer, W. G.; Hahn, D. W. *Tribol. Lett.* **2011**, *42*, 301−310.
(31) Goncalves, L. M.; Alpuim, P.; Rolo, A. G.; Correia, J. H. *Thin Solid Films* **2011**, *519*, 4152−4157.
(32) Balitskii, O. A.; Savchyn, V. P.; Yukhymchuk., V. O. *Semicond. Sci. Technol.* **2002**, *17*, L1−L4.
(33) Pérez León, C.; Kador, L.; Allakhverdiev, K. R.; Baykara, T.; Kaya, A. A. *J. Appl. Phys.* **2005**, *98*, 103103.
(34) Yoshida, H.; Nakashima, S.; Mitsuishi, A. *Phys. Stat. Sol. B* **1973**, *59*, 655−666.
(35) Baidullaeva, A.; Vlasenko, Z. K.; Dauletmuratov, B. K.; Kuzan, L. F.; Mozol, P. E. *Semiconductors* **2005**, *39* (4), 381−384.
(36) Leapman, R. D.; Grunes, L. A.; Fejes, P. L. *Phys. Rev. B* **1982**, *26* (1), 614−635.
(37) Panzer, G.; Egert, B.; Schmidt, H. P. *Surf. Sci.* **1985**, *151* (2−3), 400−408.
(38) Herzog, W.; Schwarz, M.; Sixl, H.; Hoppe, R. *Z. Phys.: Condens. Matter* **1988**, *71*, 19−22.